2009

Simulations of Aerodynamic Damping for MEMS Resonators

Xiaohui Guo
Purdue University

Alina A. Alexeenko
Purdue University - Main Campus, alexeenk@purdue.edu

39th AIAA Fluid Dynamics Conference
22 - 25 June 2009, San Antonio, Texas

AIAA 2009-3581

Simulations of Aerodynamic Damping for MEMS Resonators

Xiaohui Guo* and Alina A. Alexeenko †

Purdue Universtiy, West Lafayette, IN, 47906, U.S.A.

Aerodynamic damping for MEMS resonators is studied based on the numerical solution of Boltzmann-ESBGK equation. A compact model is then developed based on numerical simulations for a wide range of Knudsen numbers. The damping predictions are compared with both Reynold equation based models and several sets of experimental data. It has been found that the structural damping is dominant at low pressures (high Knudsen numbers). For cases with small length-to-width ratios and large vibration amplitudes, the three-dimensionality effects must be taken into account. Finally, an uncertainty quantification approach based on the probability transformation method has been applied to assess the influence of pressure and geometric uncertainties. The output probability density functions (PDF) of the damping ratio has been studied for various input PDF of beam geometry and ambient pressure.

Nomenclature

b	cantilever width, m
c_f	damping coefficient, $N \cdot sm^{-1}$
C_p	specific heat, $J(kgK)^{-1}$
E	Young's modulus, GPa
f, f^0	velocity distribution function
f	frequency, Hz
$\mathbf{F}$	external force, N
F, F_0	damping force, N
g, g^*	gap height, m
j	complex unit, $j^2 = -1$
J	Jacobian
k	Boltzmann constant
k	thermal conductivity, $W(mK)^{-1}$
Kn	Knudsen number
L	cantilever length, m
L_{ref}	characteristic length, m
M	mass of the cantilever, kgm^{-1}
n	molecular number density, m^{-3}
Pr	Prandtl number
p,p_{ij}	pressure/pressure tensor, Pa
$p(x)$	probability density function of x and y
$P(x)$	cumulative probability distribution function of X
q	complex frequency variable
Q	quality factor
Q_{pr}	relative flow rate coefficient
r^2	Pearson r^2
R	specific gas constant, $J(Kkg)^{-1}$

*Research Assistant, xguo@purdue.edu.
†Assistant Professor, AIAA Senior Member, alexeenk@purdue.edu.

t	time, s
t	cantilever thickness, m
T	temperature, K
$\mathbf{v}$, u, v, w	molecular velocity, ms^{-1}
$\mathbf{v}'$, u', v'	thermal velocity, ms^{-1}
$\mathbf{v}_0$, u_0, v_0	bulk velocity, ms^{-1}
v_m	velocity magnitude in the polar coordinate
v_s	cantilever speed, ms^{-1}
$\mathbf{x}$, x, y	Cartesian coordinates, m
x_1, x_2	independent variables of the squeeze-film damping model

Greek

β_0, β_1	linear regression coefficients
χ^2	chi-squared test (distribution)
ϕ	angle in the polar coordinate, rad
γ	ratio of specific heats ($= 1.4$)
γ_n	coefficient of the n^{th}-mode vibration
λ_{ij}	coefficient matrix in ESBGK
λ	molecular mean-free-path, m
μ	viscosity, $kg(ms)^{-1}$
ω	viscosity power coefficient
ω_n	angular frequency of the n^{th}-mode vibration, rad/sec
ρ	density, kgm^{-3}
σ	tangential momentum accommodation coefficient
σ_T	thermal accommodation coefficient of gas
τ_g	relaxation time, s
ζ_n	damping ratio of the n^{th}-mode vibration

Subscript

A	ambient
g	gas
s	solid

Abbreviations

BGK	Bhatnagar-Gross-Krook
CADP	cantilever array discovery platform
CDF	cummulative density function
DSMC	direct simulation Monte Carlo
ES-BGK	ellipsoidal-statistical BGK
MEMS	micro-electro-mechanical systems
NSSJ	Navier-Stokes slip jump
PDF	probability distribution function
PTM	probabilistic transformation method
RF	radio frequency
SFD	squeeze-film damping

I. Introduction

Predictions of gas forces on moving microstructures are of great importance in the design of MEMS.[1–3] In such microsystems the gas damping becomes increasingly significant as compared to structural damping due to increased surface-to-volume ratio.[4–6] In particular, the modeling of squeeze-film damping (SFD) of microstructures at a wide range of pressures is challenging due to the breakdown of conventional fluid dynamic models in the rarefied flow regime. The squeeze-film damping force is generated due to a small pressure difference between the top and bottom surfaces of a moving structure . The microsystems are often operating at high Knudsen number (Kn) conditions, where the molecular mean-free-path, λ, is comparable to the size of problem characteristic length.

For an oscillating beam, the damping ratio, ζ, and Quality factor, Q, of its n^{th} vibration mode are defined as following,[7]

$$\zeta_n = \frac{1}{2Q} = \frac{c_f}{2\rho_s bt\omega_n} \quad (1)$$

$$c_f = \frac{F}{v_s L} \quad (2)$$

$$\omega_n = \gamma_n^2 \sqrt{\frac{EI}{\rho_s bt L^4}} \quad (3)$$

where b is the beam width, t is the thickness and L is the length, E and I ($= bt^3/12$) refer to the Young's modulus and area moment of inertia of the cantilever, ρ_s is the mass density of structure. For a cantilever beam, the n^{th} natural resonant frequency of vibration ω_n is given by its characteristic function where γ_n are 1.8751, 4.9641 and 7.8548 for the first three modes of fixed-free cantilevers, and are 4.7300, 7.8532 and 10.9956 for the first three modes of fixed-fixed (clamped) beams. As shown in equation (1), the quality factor, Q_n, increases proportionally with the resonant frequency, ω_n, for the same damping force c_f.

The Reynolds equation has been widely used to describe gas motion of the squeeze-film damping problem in the continuum flow regime. In general, such modeling assumes a rigid plate, small gas size, small structural displacement and small pressure variation. Under the these assumptions, the Reynolds equation reduces to

$$\frac{\partial(\rho g)}{\partial t} = \nabla \cdot \left(\frac{\rho g^3}{12\mu} Q_{pr} \nabla p \right) \quad (4)$$

where g is the gap height, ρ is the gas density, p is the pressure, μ is the viscosity, and Q_{pr} is the relative flow rate coefficient to be specified.

There are a number of gas damping models and correlations valid for certain geometries and Knudsen number ranges. For example, Veijola et al[8] have developed an analytical model based on unsteady Reynolds equation with inertia effects. The model assumes small gap height and pressure changes and applies the trivial pressure boundary condition at the beam edges. A modified Reynolds equation model has been developed by Gallis and Torczynski,[9] in which they proposed a SFD correlation based on Navier-Stokes slip jump (NSSJ) and direct simulation Monte Carlo (DSMC) methods to extend RE into the slip flow regime. By employing DSMC calculations and considering non-trivial boundary conditions, their predictions significantly improves the accuracy of Reynolds equations. However, as it is known that Reynolds equation is only valid at low Knudsen numbers, predictions bases on both models may not be correct for highly rarefied cases. In addition, the stochastic DSMC method requires large computational cost at low Reynolds numbers.

In the current work, we propose a squeeze-film damping model based on numerical solution of deterministic Boltzmann equation with ESBGK collision term. The model is examined by a number of statistical goodness-of-fit tests. Then, the damping predictions are compared with both Reynolds equation based models and experimental data. The importance of the structural damping at high Knudsen numbers is discussed as well as effects of cantilever/squeeze-film length-to-width ratio and vibration amplitude. Finally, the output PDF of the damping coefficient are studied with respect to input PDF of the gap size and the ambient pressure using the probabilistic transformation method (PTM).

II. Modeling Approach

The quasi-steady two-dimensional Boltzmann equation for the velocity distribution function, f, is given as,

$$u\frac{\partial f}{\partial x} + v\frac{\partial f}{\partial y} = \frac{f_0 - f}{\tau_g} \quad (5)$$

where u and v are the gas molecular velocities in x and y direction, respectively, $1/\tau_g$ is the collision frequency, and f_0 is the equilibrium distribution function. The ellipsoidal statistical Bhatnagar-Gross-Krook (ES-BGK) model[10] is employed in the collision relaxation term. The computational domain and boundary conditions are shown in figure 1. The geometric parameters and flow conditions are specified in table 1.

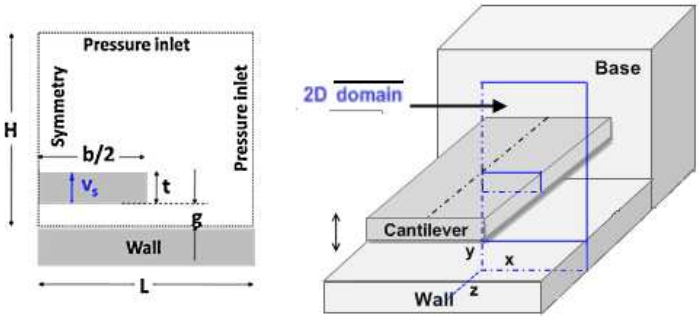

Figure 1. Schematic of computational domain and boundary conditions for squeeze-film damping simulations.

Table 1. Microcantilever geometry and flow conditions.

Property	Symbol	Nominal value
Cantilever length	L	$500.0 \times 10^{-6} m$
Cantilever width	b	$18.0 \times 10^{-6} m$
Cantilever thickness	t	$2.25 \times 10^{-6} m$
Gap height	g	$[1.0, 1.2, 1.4, 1.6, 1.8] \times 10^{-6} m$
Velocity	v_s	$< 10 m/s$
Frequency	f	$10^4 - 10^6 Hz$
Amplitude	A	approx. $10^{-9} m$
Gas	(N_2, O_2)	Air
Viscosity	μ	$1.78 \times 10^{-5} Pa \cdot s$
Temperature	T	$295K$
Pressure	P_A	$10^{-3} - 10^2 Torr$
TMAC	σ	1.0

The governing equation is solved numerically using a *Fortran-90* code developed by authors[11,12] based on the finite volume/discrete ordinate method. A second-order upwinding scheme is applied in the physical space and a sixteenth-order Gauss-Hermite quadrature is applied to velocity magnitude discretization. Grid resolution of $0.25 \mu m$ is chosen based on the grid convergence study. The domain size used in computations ensures a maximum pressure difference less than 3.0% at $Kn = 50.0$.

A closed form SFD correlation is developed based on a total number of fifty quasi-steady two-dimensional ESBGK simulations. The form and parameters are given as,

$$c_f(x_1, x_2) = \frac{F}{v_s L} = \frac{A x_1^c}{1 + B x_1^d x_2^e} \cdot t \tag{6}$$

where $A = 10.39$, $B = 1.374$, $c = 3.100$, $d = 1.825$ and $e = 0.9660$, F is the gas force, v_s is the cantilever velocity, x_1 is the ratio of the beam width to the gap height, b/g, x_2 is the gap-based Knudsen number, $Kn^{(b)}$ and t is the cantilever thickness. The correlation is examined by the goodness-of-fit, and the statistical results are listed in table 2.[13] It suggests that new SFD correlation fits very well with the ES-BGK

computations.

Table 2. Statistical analysis of the ESBGK-based compact model.

Property	Symbol	Value
Chi-square test	χ^2	1.058
Pearson's r^2	r^2	0.9980
Root mean square deviation	RMSD	7.809×10^{-4}
Mean absolute deviation	MAD	3.997×10^{-4}
Mean scaled absolute deviation	MSAD	6.085×10^{-3}
Root mean squared scaled deviation	RMSSD	3.281×10^{-2}
Mean deviation	MD	9.217×10^{-6}
Linear regression coefficients	β_0	1.315×10^{-4}
	β_1	0.989

Comparison of the quality factor for predictions of compact model, Eq. (6), and the Reynolds equation based models are shown in figure 2 for Kn ranging from 0.05 to 500 for a width-to-gap height ratio of 10.0.

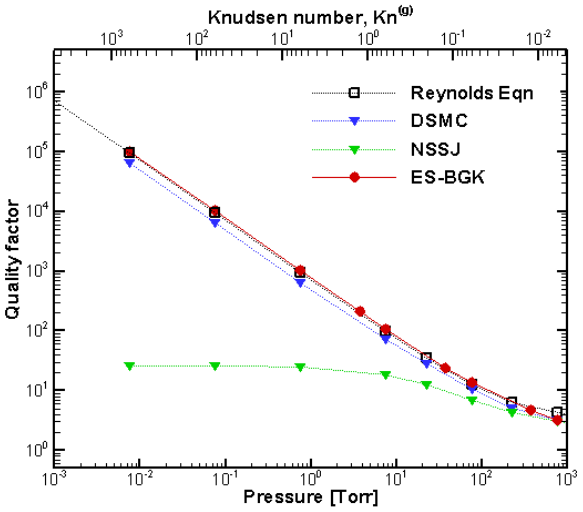

Figure 2. Comparisons of Quality factors for Mode-3,[8,9]

III. Results and Discussion

III.A. Effects of structural damping

The compact damping model is compared to experimental data by Ozdoganlar[14] as shown in figure 3. The predicted quality factor values agree very well with both sets of experimental data for pressure ranging from $5.0 Torr$ ($= 0.0066 atm$) to 1000.0 Torr ($= 1.32 atm$). However, as pressure decreases, the deviation between predictions and experimental data increase.

It is noticed that there are two major reasons that cause the deviation. First, at extremely low pressures, the beam vibration is affected by interference due to neighboring cantilevers. The neighbor effects in the micro-cantilevers arrays studied experimentally play a significant role when the molecular mean-free-path is considerably large compared to the distance between two individual beams. Second, the measured quality factor includes both structural and gas damping,

$$Q_{tot}^{-1} = Q_{structure}^{-1} + Q_{gas}^{-1} \tag{7}$$

$$\zeta_{tot} = \zeta_{structure} + \zeta_{gas} \tag{8}$$

where the subscripts "tot", "structure" and "gas" refer to the total, structural and gas quality factor or damping ratio. As noted in reference,[14] the quality factors for the same micro-cantilever cross section at different gap heights converge to a constant value at low pressures. The structural damping is independent of the gas size and is negligible compared to the gas damping at moderate and atmospheric pressures. However, at low pressures, both structural and gas damping must be taken into account.[1] As shown in figure 3, the total measured damping ratio, ζ_{tot}, at pressures $P_A < 0.1Torr$ $(1.3e-4atm)$ is dominated by the structural damping. Here, we assume that the structural damping ratio equals to the value, to which the experimental measurements of different gap heights collapse at low pressures. When the structural damping is subtracted from the total measured value as shown in figure 3, the agreement between gas damping model and experimental data becomes very close even at low pressures. A similar example[15] can be found in figure 4, where the cantilever has a much larger aspect ratio, $b/g = 36.4$, than cases shown in figure 3. It shows again that the structural damping must be taken into account at low pressures.

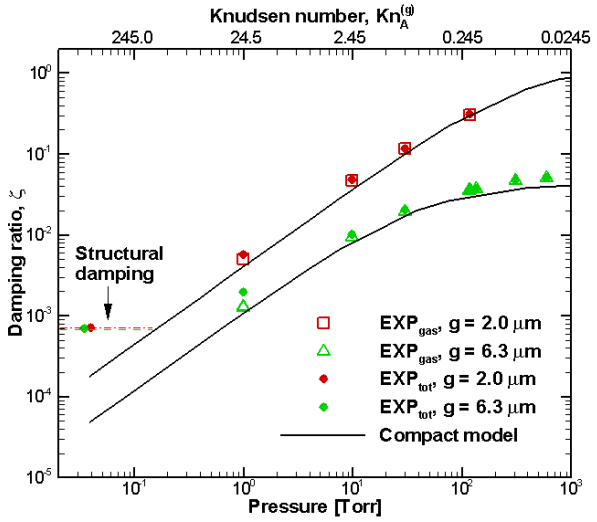

Figure 3. Comparison of predictions by the ESBGK-based compact model and experimental data in reference,[14] $g_0 = [6.3,\ 2]\mu m$, $b = 20\mu m$, $t = [2.5,\ 2.25]\mu m$, $L = 300\mu m$.

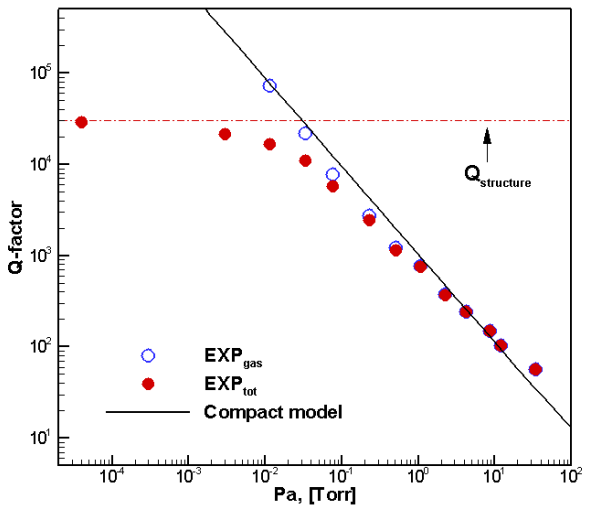

Figure 4. Comparison of predictions by the ESBGK-based compact model and experimental data in reference,[15] $g_0 = 1.1\mu m$, $b = 40\mu m$, $t = 1.8\mu m$, $L = 300\mu m$.

III.B. 3D Flow Effects

In figure 5, good agreement has been observed between compact model predictions and experimental data by J. Lee et[16] for the first three vibrational modes. The cantilever has an aspect ratio, $b/g = 12.9$, and the vibrational amplitude is less than $1nm$, i.e. the shift of modal frequencies is negligible. As the length-to-width ratio is very large, $L/b >> 1$, the damping force variation across the cantilever can be neglected. Therefore, the assumption that the damping has a single-degree-of-freedom is rational for this case, where $L/b = 250$.

In contrast, when the length-to-width ratio decreases, the multiple-degrees-of-freedom effects and gas flow three-dimnesionality need to be taken into account. The compact model that is based on the two-dimensional simulations with b/g as the only geometry input parameter may not be applicable. For example, it is found in figure 6 that the model predictions under-estimate the quality factor, or over-estimate the damping ratio, as compared to experimental data given in reference.[1] In this case, the aspect ratio of the cantilever is 37.6 and the length-to-width ratio is only 1.25. A description of the squeeze-film damping problem with multiple degrees of freedom would require a model not only dependent on b/g, but also on L/b and t/g.

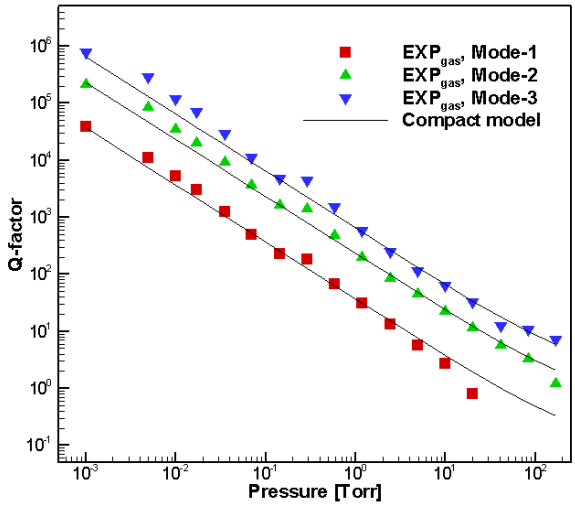

Figure 5. Comparisons of predictions by the ESBGK-based compact model and experimental data by Lee et al,[16] $L = 500\mu m$, $b = 18\mu m$, $g_0 = 1.4\mu m$, $t = 2.25\mu m$, $\rho_s = 2.33e+3\ kg \cdot m^{-3}$, $E = 160GPa$.

III.C. Effects of uncertainty

The probabilistic transformation method (PTM) evaluates the probability density function (PDF) of the system output by multiplying the input PDF by the Jacobian of the inverse function.[17]

Let Y be a continuous random variable. Then the probability and the corresponding PDF of Y are denoted as $P(Y)$ and $p(y)$, respectively.[13] For each number y, the cumulative distribution function (CDF), $F(y)$, is defined as,

$$\begin{aligned} F(y) &= P(Y < y) \\ &= \int_{-\infty}^{y} p(y_i) \cdot dy_i \end{aligned} \tag{9}$$

By substituting $Y = f(X)$ and $x = f^{-1}(y)$ into above, it gives,

$$\begin{aligned} P(Y < y) &= P[f(X) < y] \\ &= P[X < f^{-1}(y)] = P(X < x) \end{aligned} \tag{10}$$

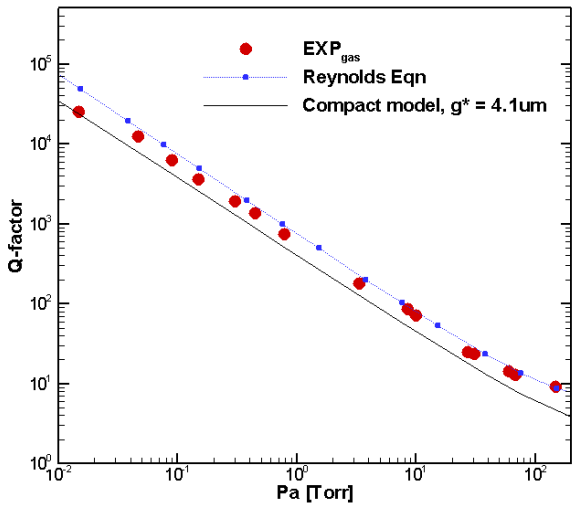

Figure 6. Comparisons of predictions by the ESBGK-based compact model and experimental data in reference,[1] $L = 193\mu m$, $b = 154\mu m$, $g_0 = 4.1\mu m$, $t = 5.7\mu m$, $\rho_s = 19.3e+3\ kg \cdot m^{-3}$, $E = 78GPa$, Mode-1.

and,

$$\begin{aligned} P(X < x) &= \int_{-\infty}^{x} p(x_i) \cdot dx_i \\ &= \int_{-\infty}^{y} p(x_i) \cdot \ |J_{x,y}| \cdot dy_i \end{aligned} \tag{11}$$

where $J_{x,y}$ is the Jacobian of the inverse function from x to y. Comparing equation (9) and (11), the formula for PTM is obtained as following,

$$p(y) = p(x) \cdot |J_{x,y}| \tag{12}$$

To ensure that the probabilistic transformation is bijective, the following two constraints need to be satisfied:

1. The transformation between y and x should be a bijective mapping;
2. The determinant of Jacobian should be non-zero (or "not null").

Considering a squeeze-film-damping problem with the schematic shown in figure 1, where the length, width and thickness of the cantilever are referred as l, b and t, the gap height is g, the simulation domain size are L by H. The compact model based on rarefied gas dynamics simulations is given as,

$$c_f = \frac{A x_1^c}{1 + B \cdot x_1^d x_2^e} \cdot t \tag{13}$$

where coefficients $A = 10.39$, $B = 1.374$, $c = 3.100$, $d = 1.825$ and $e = 0.966$. x_1 and x_2 are independent variables. It can be shown that the transformation satisfies both constraints given earlier. Therefore, the output PDF of the damping force, $P[c_f(x_1, x_2)]$, can be obtained from the known input PDF based on PTM shown in equation (12). For a single-degree-of-freedom problem, it gives,

$$p[c_f(x_1)] = p(x_1) \cdot |J_{x_1,cf}| \tag{14}$$

$$p[c_f(x_2)] = p(x_2) \cdot |J_{x_2,cf}| \tag{15}$$

where,

$$J_{x_1,cf} = \frac{\partial x_1}{\partial c_f} = \left(\frac{\partial c_f}{\partial x_1}\right)^{-1} = \frac{1}{J_{cf,x_1}} \tag{16}$$

$$J_{x_2,cf} = \frac{\partial x_2}{\partial c_f} = \left(\frac{\partial c_f}{\partial x_2}\right)^{-1} = \frac{1}{J_{cf,x_2}} \tag{17}$$

and,

$$\frac{\partial c_f}{\partial x_1} = \frac{Ac \cdot x_1^{c-1} + (c-d)ABx_2^e \cdot x_1^{c+d-1}}{(1+Bx_1^d x_2^e)^2} \cdot t \tag{18}$$

$$\frac{\partial c_f}{\partial x_2} = -\frac{ABex_1^{c+d}x_2^{e-1}}{(1+Bx_1^d x_2^e)^2} \cdot t \tag{19}$$

Further, the PDF of the damping force can be expressed in terms of the PDFs of physical quantities by applying the chain rule. For example, assuming the input PDF of the gap height, $p(g)$, is known. Since $x_1 = b/g$, it gives that,

$$\begin{aligned} p(c_f) &= [p(g) \cdot |J_{g,x_1}|] \cdot |J_{x_1,cf}| \\ &= p(g) \cdot \frac{g^2}{b} \cdot |J_{x_1,cf}| \end{aligned} \tag{20}$$

A similar approach can be used in analyzing the effects of input PDF of the ambient pressure, $p(p_A)$, on the output PDF of damping force. Recall the expression for x_2,

$$x_2 = x_2(p_A) = \frac{\mu}{p_A b}\sqrt{\frac{\pi RT}{2}} \tag{21}$$

So,

$$\begin{aligned} p(c_f) &= [p(p_A) \cdot |J_{p_A,x_2}|] \cdot |J_{x_2,cf}| \\ &= p(p_A) \cdot \frac{p_A^2 b}{\mu}\sqrt{\frac{2}{\pi RT}} \cdot |J_{x_2,cf}| \end{aligned} \tag{22}$$

Assuming the input PDF has a normal distribution $N(\mu, \sigma^2)$, the output PDF can be obtained from equation (20). Take for example, $\mu = g_0 = 1.4e-6$ and $\sigma^2 = (0.25e-6)^2$. The input and output PDFs at two Knudsen numbers, $Kn^{(b)} = 3$ and 0.003, can be found in figure 7, 8(a) and 8(b), respectively. The conditions for different cases can be found in table 3.

Since the normal distribution is generated by random numbers, the result is depending on the sample size, N. Based on a sensitivity study, a sample size of $1e+6$ is used. In general, the output PDF after the probabilistic transformation is an nonparametric distribution, which can be described by its first four moments: mean, standard deviation (STD), skewness and kurtosis.

It is noticed that the output mean value, c_{f0}, is not the same as that corresponding to the input mean. In fact, c_{f0} is to the right of $c_f(g_0)$ on the curve of the output PDF. In figure 9, it shows that as Knudsen number decreases, the relative difference increases from $2 \approx 5\%$ to $5 \approx 13\%$.

A similar approach has been done in studying the output PDF of damping due to uncertainties in the ambient pressure, as shown in figure 10 and 11. Different from the cases with uncertainties in the gap size, the shifts between c_{f0} and $c_f(p_{A0})$ are negligible. For gap size varying from 1 to $2\mu m$ shown in figure 12, the results are consistent.

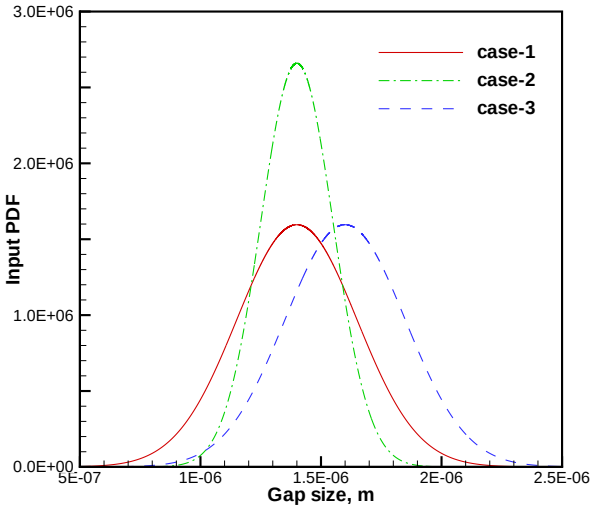

Figure 7. Input PDF of the gap size.

Table 3. Statistical analysis of the ESBGK-based compact model.

Case	mean, μ	STD, σ
gap size, g		
case-1	$1.4\mu m$	$0.25\mu m$
case-2	$1.4\mu m$	$0.15\mu m$
case-3	$1.6\mu m$	$0.25\mu m$
ambient pressure, p_A		
case-4	$0.92Torr$ $(122.5Pa)$	$0.23Torr$ $(30.6Pa)$
case-5	$0.92Torr$ $(122.5Pa)$	$0.14Torr$ $(18.4Pa)$
case-6	$1.05Torr$ $(140.0Pa)$	$0.23Torr$ $(30.6Pa)$

IV. Conclusions

Numerical investigations of aerodynamic damping in MEMS resonators are carried out using deterministic ES-BGK simulations. A new compact damping model based on the simulations is then formulated. Model predictions show good agreement with previous numerical models at low Knudsen numbers. Comparison with experimental data shows that the structural damping must be subtracted from the total damping measurements. For different sets of experimental data, the compact model gives good agreement. However, for cases where the length-to-width ratio is very small, multiple-degrees-of-freedom effects must be taken into account. Using the compact model, it is possible to study the effects of uncertainties on the damping, e.g. due to the uncertainties in the geometric parameters such as squeeze-film gap size, or the ambient pressure. The application of the probability transformation method for uncertainty quantification, shows that there is a significant difference between the output mean value of damping and the value corresponding to the mean input gap size.

Acknowledgments

The work is supported by NNSA Center for Prediction of Reliability, Integrity and Survivability of Microsystems at Purdue University under Contract Number DE-FC52-08NA28617.

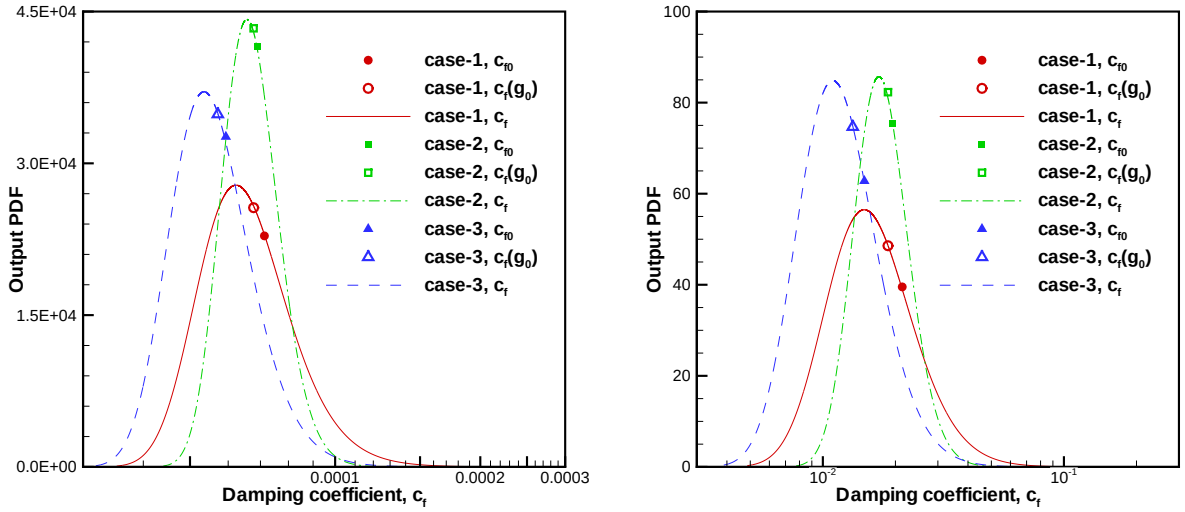

(a) $Kn = 3$ (b) $Kn = 0.003$

Figure 8. Output PDF of the damping coefficient due to uncertainties in the gap size.

References

[1]Sumali, H., "Squeeze-film damping in the free molecular regime: model validation and measurement on a MEMS," *Journal of Micromechanics and Microengineering*, Vol. 17, No. 11, 2007, pp. 2231–2240.

[2]Mohite, S. S., Sonti, V. R., and Pratap, R., "A Compact Squeeze-Film Model Including Inertia, Compressibility, and Rarefaction Effects for Perforated 3-D MEMS Structures," *Microelectromechanical Systems, Journal of*, Vol. 17, No. 3, 2008, pp. 709–723.

[3]Bao, M. and Yang, H., "Squeeze film air damping in MEMS," *Sensors and Actuators A: Physical*, Vol. 136, No. 1, 2007, pp. 3–27.

[4]Chang, K. M., Lee, S. C., and Li, S. H., "Squeeze film damping effect on a MEMS torsion mirror," *Journal of Micromechanics and Microengineering*, , No. 5, 2002, pp. 556.

[5]Corman, T., Enoksson, P., and Stemme, G., "Gas damping of electrostatically excited resonators," *Sensors and Actuators A: Physical*, Vol. 61, No. 1-3, 1997, pp. 249–255.

[6]Pan, F., Kubby, J., Peeters, E., Tran, A. T., and Mukherjee, S., "Squeeze film damping effect on the dynamic response of a MEMS torsion mirror," *Journal of Micromechanics and Microengineering*, Vol. 8, 1998, pp. 200–208, [1] [2].

[7]Meirovitch, L., *Principles and Techniques of Vibrations, 2nd ed.*, Prentice Hall, 2000.

[8]Veijola, T., "Compact models for squeezed-film dampers with inertial and rarefied gas effects," *Journal of Micromechanics and Microengineering*, Vol. 14, No. 7, 2004, pp. 1109–1118.

[9]Gallis, M. A. and Torczynski, J. R., "An improved Reynolds-equation model for gas damping of microbeam motion," *Journal of Microelectromechanical Systems*, Vol. 13, No. 4, 2004, pp. 653–659.

[10]Mieussens, L. and Struchtrup, H., "Numerical comparison of Bhatnagar–Gross–Krook models with proper Prandtl number," *Physics of Fluids*, Vol. 16, No. 8, 2004, pp. 2797–2813.

[11]Guo, X., Singh, D., Murthy, J., and Alexeenko, A. A., "Gas-phonon interaction model for subcontinuum thermal transport simulations," 2008.

[12]Singh, D., Guo, X., Alexeenko, A. A., and Murthy, J., "Modeling of subcontinuum thermal transport across semiconductor-gas interfaces," *proceedings of Summer Heat Transfer Conference*, Vol. 56427, Florida, USA, 2008.

[13]Devore, J. L., *Probability & Statistics for Engineering & the Sciences, 6th ed.*, Brooks Cole, 2004.

[14]Ozdoganlar, O. B., Hanshce, B. D., and Carne, T. G., "Experimental modal analysis for micro-electro-mechanical systems," *Society for Experimental Mechanics*, Vol. 45 (6), 2005.

[15]Zook, J., Burns, D., Guckel, H., Sniegowski, J., Engelstad, R., and Feng, Z., "Characteristics of polysilicon resonant microbeams," *Sensors and Actuators A: Physical*, Vol. 35, No. 1, 1992, pp. 51–59.

[16]J.W. Lee, R. Tung, A. R. and Sumali, H., "Submitted," 2009.

[17]Kadry, S., "On the generalization of probabilistic transformation method," *Applied Mathematics and Computation*, Vol. 190, No. 2, 2007, pp. 1284–1289.

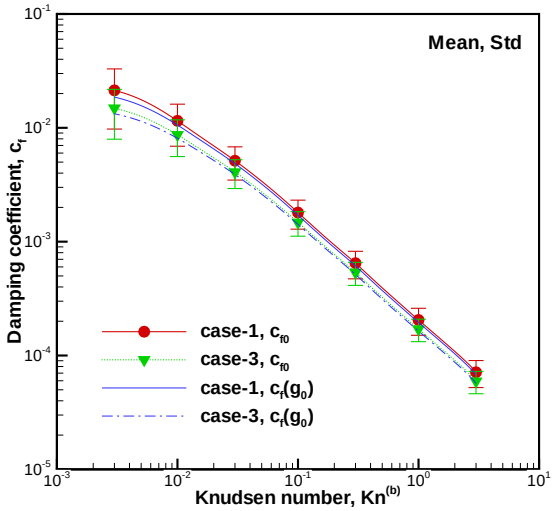

Figure 9. Skewness effects due to uncertainties of the gap size.

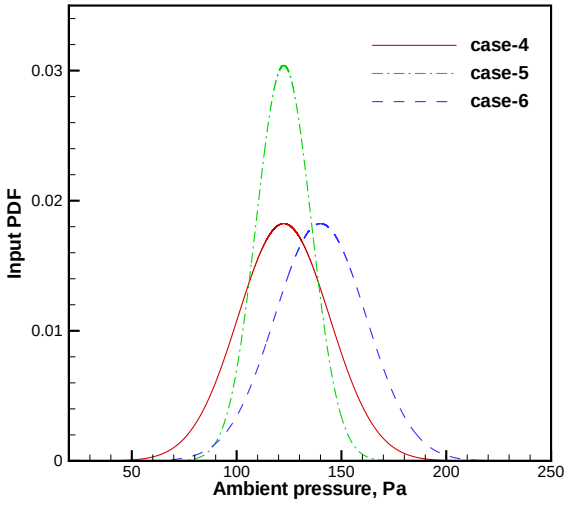

Figure 10. Input PDF of the ambient pressure, $g = 1.4\mu m$.

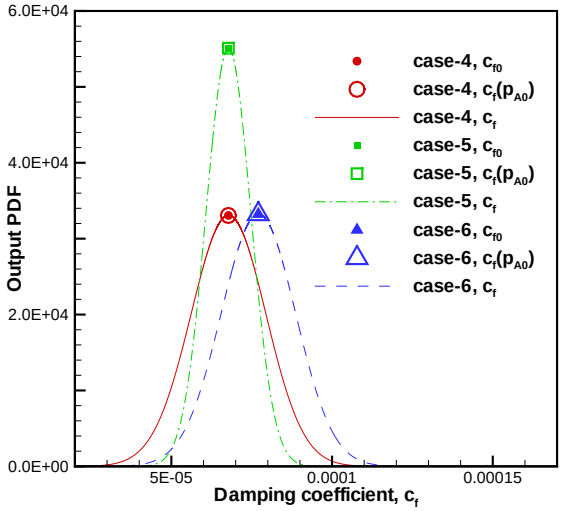

Figure 11. Output PDF of the damping coefficient due to uncertainties in the ambient pressure, $g = 1.4\mu m$.

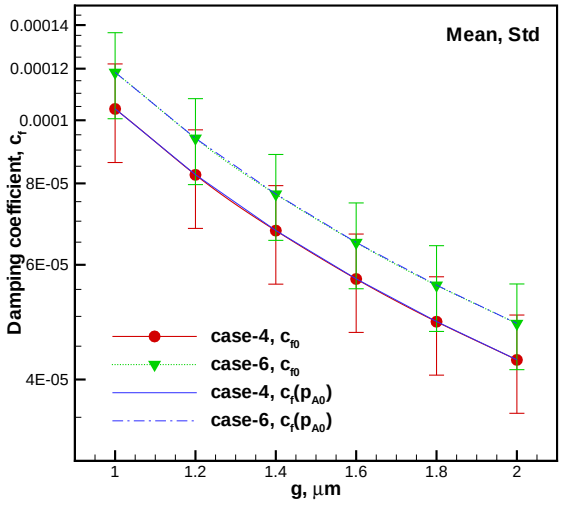

Figure 12. Skewness effects due to uncertainties of the ambient pressure.